Long Wavelength Single Photon Like Driven Photolysis Via Triplet-Triplet Annihilation

Gang Han (gang.han@umassmed.edu)
University of Massachusetts-Medical School
Ling Huang
University of Massachusetts Medical School
Le Zeng
University of Massachusetts Medical School
Yongzhi Chen
University of Massachusetts Medical School
Nuo Yu
University of Massachusetts Medical School
Lei Wang
University of Massachusetts Medical School
Kai Huang
University of Massachusetts Medical School
Yang Zhao
University of Massachusetts Medical School

Research Article

Keywords: Photolysis, nanoparticles , long wavelength light , triplet-triplet annihilation

Posted Date: September 2nd, 2020

DOI: https://doi.org/10.21203/rs.3.rs-69848/v1

Abstract

Photolysis has enabled the occurrence of numerous discoveries in chemistry, drug discovery and biology. However, there is a dearth of efficient long wavelength light mediated photolysis. Here, we report general and efficient long wavelength single photon method for a wide array of photolytic molecules via triplet-triplet annihilation photolysis (TTAP). This method is versatile and "LEGO"-like. The light partners (the photosensitizers and the photolytic molecules (PPG-Xs)) can be energetically matched to adapt to an extensive range of electromagnetic spectrum wavelengths and the diversified chemical structures of photoremovable protecting groups (PPGs), photolabile linkages, as well as a broad array of targeted molecules. Our TTAP not only surpasses reaction yields, it also resolves the photodamage problem of the existing photolysis methods, regardless of whether they are a single photon or multiple photons associated. Furthermore, we developed ambient air-stable, TTAP nanoparticles to illustrate the biological promise of TTAP “LEGO” systems.

Main Text

Photolysis is a chemical reaction in which a chemical compound is broken down by light to allow for non-invasive control of the release and activation of targeted molecules. Due to the unique and precise spatiotemporal controllability, the use of photolysis has been a powerful approach that has vast applications from organic synthesis, drug discovery to numerous biological areas, such as developmental biology, neuromodulation, as well as cancer treatments. In general, a photolytic molecule (PPG-X) consists of three key components: a target molecule, a photolabile linkage and a photoremovable protecting group (PPG). In photolysis, PPG absorbs high-energy photons and then transitions to an excited state, causing photolabile linkage to break down, leading targeted molecules to be released. Unfortunately, most of the existing PPGs, such as coumarin (Cou), anthracene (An) and perylene (Py), boron-dipyrromethene (BDP) groups only respond to high energy short wavelength light excitation for subsequent single photon photolytic reactions (**Fig 1A**)1. However, the use of short wavelength light for photolysis has inherent drawbacks. For instance, the shallow penetration of such short wavelength light through colored reaction solvents or media leads to poor photolytic reaction yields, especially in large-scale chemical reactions 2. In addition, short wavelength photons cause the rapid photodamage and photobleaching of PPGs1, 2. Moreover, in regard to photolysis applications in biology, the term "photouncaging" has been coined to describe the technique of using light to remove the PPGs and activate biological compounds so as to noninvasively probe different biological processes, neuronal connections, as well as to develop disease treatments 3. However, photouncaging using conventional short wavelength light also comes along with a series of serious problems, such as inevitable phototoxicity and shallow tissue penetration depths 4. Ideally, these problems can be overcome by the use of lower energy long wavelength light (including far red light and near infrared light), which has much higher penetration depth through various media and biological tissue 5.

To date, there are only a pair of state-of-the-art long wavelength activation photolytic methods in the reported literature. For example, the femtosecond pulsed two-photon laser can be used to remove PPGs 6.

However, this process is quite inadequate for photolysis, as the two-photon absorption cross-sectional area of PPGs is quite weak and the reactions can only take place in the tiny area of the laser focal point (**Fig 1B**) 1. Meanwhile, lanthanide ion-doped upconversion nanoparticles (UCNPs)-assisted photolysis have emerged as an appealing method 7. Yet, owing to low absorption and emission cross-sections, the lanthanide ion-doped UCNPs typically suffer from the need for high power light excitation (101-104 W.cm-2) and inherently low quantum yields.8, 9 In addition, upconversion luminescence resonance energy transfer (LRET) from inorganic UCNP nanoparticles to conjugated PPGs is generally inefficient (**Fig 1C**).

In this study, we report on a highly effective and general long wavelength single photon driven photolysis method via triplet-triplet annihilation. The detailed mechanism for our triplet-triplet annihilation mediated photolysis (TTAP) is delineated in **Fig 1D**. As depicted, photosensitizers (Sens) can absorb low energy long wavelength photons, reach their singlet excited state (1[Sen]*) and subsequently populate their long-lived triplet excited state (3[Sen]*) through rapid intersystem crossing (ISC). The resultant lifetime of this photosensitizer triplet excited state is long enough to allow collisions of the targeted photolytic molecules (PPGs-X) to occur. The energy of 3[Sen]* can thus be efficiently transferred to PPGs-X. Consequently, the triplet-triplet annihilation (TTA) of *[PPGs-X]1 drives photolytic reactions to take place, thus breaking down the photolabile linkage and releasing and activating the targeted molecules. Because of the much greater light absorption of photosensitizers than PPGs themselves and the highly efficient triplet-triplet energy transfer (TTET) from photosensitizers to PPGs-X, we envision our long wavelength single photon driven TTAP method is anticipated to outperform the existing short-wavelength single photon direct activation and the abovementioned long wavelength activation methods.

In particular, in the proposed TTAP process, there are two general rules to design effective TTAP “LEGO” systems: (1) the PPGs should have a lower laying triplet excited state than that of the triplet excited state of the photosensitizer (3[PPGs]* < 3[Sen]*), allowing the efficient TTET process to occur from Sen to PPGs; (2) the doubled energy of the triplet excited state of the PPGs should be higher than that of the singlet excited state of the PPGs (2 ´ 3[PPGs]* > 1[PPGs]*), enabling the ultimate TTA to take place (**Fig 1D**).10-12

To verify our hypothesis, we began our TTAP investigation with a widely used PPG from an ultraviolet light absorbing coumarin group (T1 = 2.18 eV) (**table S1**)13. Here, due to its broad presence in pharmaceuticals and natural products, in conjunction with such PPG from coumarin group, the ester bond was tested to see the feasibility of its being used for photolabile linkage to protect carboxylate (acetic acid) in compound **1**. After considering the energetic requirements of the TTAP, Ir(ppy)3 (T1 = 2.4 eV) (**table S1**) was chosen as the initial coupling photosensitizer partner (SI, **Section S3**, **Fig S2**) 14. The TTET process from Ir(ppy)3 to compound **1** was studied via Stern−Volmer photoluminescence quenching assays under oxygen-free conditions. When we titrated the Cou (compound **1**) into the Ir(ppy)3 solution, the phosphorescence decreased dramatically (**Fig S3**). The respective Stern−Volmer constants (*ksv*) were calculated to be 3.13´103 M−1. Next, when combining the Ir(ppy)3 with compound **1**, we observed the photolytic product in 73% of the yield under the blue light illumination at characteristic absorption of Ir(ppy)3 (476 nm, LED, 20 mW/cm2). In contrast, in the absence of Ir(ppy)3, no photolytic product was

observed under such blue light irradiation since the PPG of the coumarin group requires ~360 nm ultraviolet short wavelength light direct activation (**table S4**). This experiment clearly validated the feasibility of our proposed TTAP concept.

Inspired by the above mentioned TTAP experimental results, we continued to examine whether this TTAP concept is general enough to be adapted to a wide spectrum of electron- magnetic wavelengths (**Fig 1G-1H**). To do so, we tested a series of long wavelength absorbing sensitizers, ranging from green (PtOEP), far-red (PdTPBP) to near infrared light (PtTNP) **(Fig 1E**), as well as a broad array of PPGs (An, Py and BDP) (**Fig 1F**). Through extensive analysis of the photophysical properties (SI, **Section S3, table S2-S3**), we identified a family of potential TTAP light partners based on the energetic match among these sensitizers and PPGs. These new TTAP pairs are: (1) PtOEP: An; (2) PtOEP: Py; (3) PdTPBP:Py; (4) PdTPBP:BDP; (5) PtTNP:Py and (6) PtTNP:BDP. (**table S2-S3**, **Fig S2**) To further support our theoretical spectrum analysis, we then tested the Stern−Volmer constants (*ksv*) (SI, **Section S5-S7**) in regard to all of these selected combinations. As shown in **table S1**, compound **2** with PPGs of anthracene (T1 = 1.77 eV)15 and compound **8** with PPGs of perylene (T1 = 1.52 eV) 16 demonstrate significant quenching of the photoluminescence of green light absorbing photosensitizer of PtOEP (T1= 1.92 eV) (**Fig S5**, **Fig S7**). Meanwhile, for far-red light absorbing photosensitizer of PdTPBP, PPG-X of compound **7** with PPG of BDP (T1 = 1.49 eV) and PPG-X of compound **8** with PPG of perylene exhibited obvious quenching effects on the photoluminescence of PdTPBP (T1= 1.55 eV) (**Fig S9**, **Fig S10**). Moreover, regarding NIR light absorbing photosensitizer of PtTNP, compound **7** and compound **8** also show quenching effect on its photoluminescence (T1= 1.43 eV) (**Fig S11**).

Moreover, the TTA-upconversion properties were studied for these pairs. The TTA- upconversion spectra of these pairs were measured in deaerated toluene. The upconversion quantum yields (FUC) were calculated based on the established method in the literature12. **Fig S6** and **Fig S8** are the TTA-upconversion spectra of green light activated TTA-pairs of PtOEP: An (compound 2) and PtOEP:Py (compound 8) under 530 nm (20 mW/cm2) light illumination. The upconversion quantum yields are determined to be 8.7% for PtOEP: An (compound 2) and 9.5 % for PtOEP: Py (compound 8). **Fig S15a** and **Fig S15b** are TTA-UC spectra of the red light activated TTA pairs of PdTPBP:Py (compound 8) and PdTPBP:BDP (compound 7) under 650 nm (20 mW/cm2) light illumination. The upconversion quantum yields are determined to be 5.8% for PdTPBP:Py (compound 8)) and 8.4% for PdTPBP:BDP (compound 7). **Fig S15c** and **Fig S15d** are The TTA-UC spectra of the NIR light activated TTA pairs of PtTNP:Py (compound 8) and PtTNP:BDP (compound 7) under 650 nm (20 mW/cm2) light illumination. The upconversion quantum yields are determined to be 0.05 % for PtTNP:Py (compound 8) and 0.3% for PtTNP:BDP (compound 7). Furthermore, the upconversion emission for the TTA-pairs is observed to be power-dependent (**Fig S12-Fig S14**). The threshold intensities (*I*th) are determined to be 25.4mW/cm2 for PtOEP:An (compound **2**), 21.8mW/cm2 for PtOEP:Py (compound **8**), 48.1 mW/cm2 for PdTPBP:Py (compound **8**), 46.7 mW/cm2 for PdTPBP:BDP (compound **7**), 94.5 mW/cm2 for PtTNP:Py (compound **8**) and 119.8 mW/cm2 for PtTNP:BDP (compound **7**) respectively. Below the respective threshold intensity (*I*th), the upconversion intensity (*I*UC) and excitation power intensity (*I*ex) are in a quadratic relationship.

When the *I*ex exceeds the threshold intensity, the relastionship between *I*UC and *I*ex becomes linear (**Fig S12-Fig S14**).

Next, we then measured the photolysis yields of the above mentioned TTAP "LEGO" systems (**Fig. 2**). Specifically, we first tested the two green light activating TTAP pairs, including PtOEP: An (compound **2**) and PtOEP: Py (compound **8**). We found that their photolytic yield is outstanding: 83% for An containing compound **2** and 61% for Py containing compound **8** respectively under 20 mW/cm2 532nm LED light (**table S5-table S6**). In a similar manner, we also observed significant photolytic yield at 76% and 87% for our far-red light activating TTAP pairs (PdTPBP: compound **7**, PdTPBP: compound **8**) respectively under 20 mW/cm2 650 nm LED light (**table S7-table S8**). Moreover, we tested our NIR light activating TTAP candidates (PtTNP: compound **8**, PtTNP: compound **7**). Notable photolytic yield at 14.7% and 17.7% were also respectively observed under 1 h illumination of 20 mW/cm2 720 nm NIR LED light (**table S9- table S10**).

It is exciting that we further found that such low energy long wavelength activation can indeed even surpass the traditionally needed high energy short-wavelength light direct activation. This is the case because of the advantages of the TTAP in regard the intense long wavelength light absorbance of photosensitizer, the highly effective TTAP mechanism and the reduced photodamage on the photolytic molecules. For example, in the presence of the photosensitizer partner, the traditional photolytic reaction on compound **8** with blue light (445 nm, 20 mW/cm2) only leads to a 59% photolytic reaction yield. (**table S11**). In contrast, our TTAP "LEGO" system (PdTPBP: compound **8**) is able to effectively improve the photolytic yield to 87.1% for compound **8** under a far-red LED (20 mW/cm2, 650 nm). Furthermore, the photolytic quantum efficiency (QE) were calculated (QE = ε ´Fp ´FTTET´FTTA). The resulted QE gives an overall evaluation with respect to photolysis reactions, as it considers both the photolysis quantum yield of PPGs and the absorbance of sensitizers, TTET and TTA quantum yields (**Section 8 in Supporting information**, **table S12**). As a result, for the PPG of An (compound **2**), in conjunction with PtOEP, QE (TTAP) is calculated to be 1255. For the PtOEP and Py (compound 8), the QE (TTAP) is calculated to be 708. Moreover, in conjunction with PdTPBP the QE(TTAP) is calculated to be 679 for the PPG of Py (compound **8**) and QE (TTAP) is 12.3 for BDP (compound 7), respectively. In addition, the QE (TTAP) is 7.1 for the PPG of Py (compound **8**) and QE (TTAP) is 0.53 for the PPGs of BDP in conjunction with PtTNP, respectively.

Compared to conventionally used protecting groups in peptide synthesis that are involved with harsh chemical conditions such as acid/base- or redox-sensitive groups, PPGs have been emerging as a traceless and green alternative to allow "reagent-free" deprotection under light illumination17. Thus, herein we expanded our TTAP concept to a variety of amino acids such as glycine, cysteine and phenylalanine (**Fig 2**). As a result, we observed excellent low power long wavelength light driven single photon mediated deprotection for these amino acids containing target molecules. For PPGs of An for protecting glycine (compound **5**), we observed the photolytic yield is 58.4 % in conjunction with PtOEP under green LED illumination. For PPGs of Py for protecting glycine (compound **12**), in conjunction with PdTPBP and PtTNP, the photolytic yield is 89.2 %, 29.6 % respectively. For PPGs of Py for protecting

cysteine (compound **14**), when PdTPBP and PtTNP are used as photosensitizers, the photolysis yields are 81.2 % and 23.3 %. In addition, for PPGs of Py for protecting phenylalanine, with PdTPBP and PtTNP as photosensitizers, the photolytic yields are 70.9 % and 29.0 % respectively. These results demonstrated the great potential of our TTAP technology in a wide array of applications in relation to functional photocaged amino acids and peptide synthesis. (**Fig. 2**)

Having identified our TTAP "LEGO" systems enable photolytic ester bonds, we then turned our attention to evaluate the scope of this method with other typically used photolabile linkages of carbonate (compound **3**, compound **9**) and carbamate (compound **4**, compound **10**) in the alcohols and amines containing targeted molecules. We found that PtOEP: compound **3** and PtOEP: compound **4** were effectively photolyzed under green light illumination, respectively, in 72.3%, 51.0% yield. Under far red-light illumination, PdTPBP: compound **9** and PdTPBP: compound **10** were also efficiently photocleaved. The photolytic yields are 65.3%, 52.4% respectively (**Fig 2**). Moreover, NIR light activated TTAP "LEGO" s including PtTNP: compound **9** and PtTNP: compound **10**, were both compatible with this method, affording 27.8%, 29.3% photolytic yield (**Fig 2**).

In addition to the above-mentioned amino acids, we also explored the possibility of extending TTAP compatible targeted molecules to small molecule drugs in current clinical use. In particular, small molecule drugs such as anti-inflammatory and anti-tumor drugs, are known to have server systematic off-target side effects19-21. To this end, light-activatable prodrugs constitute emerging major targets for utilization in drug discovery, due to their high spatiotemporal resolution in the treatment of complex diseases22, 23. Here, we constructed a series of TTAP compatible prodrugs via the conjugation of a series of anti-nonsteroidal and anti-inflammatory drugs (naproxen, indomethacin, ibuprofen) with perylene via ester bonds (**Fig 2**). These resultant compounds (compounds **16**, **17**, **18**) were denoted as pro-naproxen, pro-indomethacin and pro-ibuprofen. In conjunction with the far-red light photosensitizer (PdTPBP) or the NIR light photosensitizer (PtTNP), we observed that pro-naproxen (compound **16**) has excellent photolytic reaction yields of 78.5% (PdTPBP) and 17.4% (PtTNP). For the pro-indomethacin (compound **17**), the photolytic reaction yield is 51.7% (PdTPBP) and 9.2% (PtTNP). In addition, the photolytic reaction yields are also found to be quite effective: 71.6% (PdTPBP), and 19.4% (PtTNP) for pro-ibuprofen (compound **18**). The carbonate photolabile linkage containing pro-cholesterol (compound **20**) was also constructed and can be selectively photolyzed in the yields of 69.4 % (PdTPBP) and 28.6 % (PtTNP) under 1 hour far-red or NIR light illumination (**Fig 2**).

Next, in order to illustrate the biological applications via TTAP, we chose chlorambucil, which is an FDA approved anti-cancer drug to evaluate the effect of cancer treatment 24. In this regard, we conjugated Py with chlorambucil to obtain pro-chlorambucil (compound **19**). Then, when PdTPBP or PdTNP were used as the coupling light partners, we observed the respective photolytic yield of 72.8% (PdTPBP) (**table S14**) and 30.4 % (PtTNP) (**table S15**). We then designed an oleylamine substituted amphiphilic polymer (PSMA-PEG-OAm) encapsulated TTAP nanoparticles to resolve the noxious di-oxygen quenching of the triplet states of Sens and PPGs-X under ambient air conditions (SI, **Section 10**). This unsaturated olefin-

modified amphiphilic polymer was found to be able to encapsulate Sens and PPG-X to form air-stable monodispersed and water soluble ultra-small sized TTAP nanoparticles (TTAP NPs) (SI, **Section S11**).

Via 1H-NMR spectra and the phosphorescence quenching experiments (**Fig S16**), we found that the unsaturated olefins can react with singlet oxygen to exhaust oxygen from the stored solution under light illumination. Due to the outstanding photolytic yield of the combination PdTPBP: compound **19**, we prepared TTAP nanoparticles (TTAP NPs) that contain PdTPBP and compound **19**. The entrapment and drug loading efficiency are measured to be 89% and 16% in TTAP NPs (SI, **Section S0**). Via TEM and DLS characterization, the TTAP NPs have ultra-small size (12.9 ± 2.6 nm, 29.7 ± 4.6 nm, respectively). Moreover, after 30 days, the size also stayed at ~30 nm via DLS, suggesting the excellent stability of TTAP NPs (**Fig S17**). Via the UV-vis absorption of TTAP NPs, we further confirmed that TTAP NPs contains PdTPBP and compound **19** (**Fig S18**). In addition, after 650 nm (20 mW/cm2) light irradiated for 30 min, we did not observe significant photobleaching, suggesting that TTAP NPs have robust photostability (**Fig S19**). We then tested the photolytic kinetic process of TTAP NPs (**SI, section 12**). After 60 min 20 mW/cm2, 650nm LED illumination, the 64% prodrug was effectively photolyzed. Moreover, the photolysis process was clearly dependent on the ON–OFF pattern of the LED excitation (**Fig S21b**). This result clearly validated the feasibility of the use of our TTAP “LEGO” system in aqueous solution under ambient air. The dose and duration of the prodrug activation can be precisely interrogated by our TTAP nanoparticles.

We then conducted *in vitro* and *in vivo* studies of our TTAP NPs. Firstly, via MTT assays, we demonstrated that TTAP NPs significantly enable the inhibition of cancer cell growth (**Fig S22**). This result suggests that via TTAP, the prodrug (pro-chlorambucil) was photolyzed and released from TTAP NPs into cancer cells, causing cancer cell death under far red-light illumination. Moreover, we evaluated the phototoxicity of PdTPBP NPs per se. However, we did not observe obvious cell death in the presence of the light, suggesting the negligible phototoxicity of PdTPBP (**Fig S23**).

Next, we went on to examine the synergistic the anti-tumor immunotherapy effect of our TTABP system in conjunction with the checkpoint blockade PD-L1 anti-body (a-PD-L1) in a bilateral model of 4T1 tumor bearing BALB/c mice 25, 26. As shown in **Fig 3A**, the tumor on the right represented the primary tumor that was subjected to the injection of TTAP NPs and the subsequent light treatment. The tumor on the left was left untreated and served to mimic a distant metastatic tumor. When the tumor on the right reached 100 mm3, TTAP NPs were intratumorally injected. After 4 hours, this tumor was exposed to NIR light (650 nm, 20 mW/cm2) for 30 min. At the 7th, 8th and 9th day, the mice were i.p. injected with the a-PD-L1 (75μg / mouse) (**Fig 3B**). The therapeutic efficacy of different treatment groups was evaluated by measuring tumor volume and weight. The volume growth rates for the tumor on the right are presented in **Fig 3C**. In group 5 (TTAP NPs + *hv*), we only observed that the right tumor volume was more suppressed than that observed in groups 1-4. In contrast, in group 6 (TTAP NPs+ *hv* + a-PD-L1), both the right and left tumor volume showed obvious reduction (**Fig 3D** and **Fig S24**). Moreover, after 15 days, the right and left tumors were isolated respectively, and then weighed the tumor mass, as shown in **Fig 3E** and **3F**, the results were consistent with tumor volume growth. These experimental results clearly demonstrated that

the TTABP mediated prodrug photolytic system potentiated the checkpoint blockade immunotherapy efficacy and promoted abscopal effects.

We next explored the mechanism by which TTAP mediated prodrug photolysis enhanced the efficacy of immunotherapy (SI, **section 14**). In particular, we first analyzed immune cell profiling in the spleen (**Fig S25a-b**, **Fig S26**). The cytotoxic CD8+ T cell and helper CD4+ T cell levels significantly increased in the treated group, as compared to those in the PBS treatment group (group 1). After stimulation with PMA/ionomycin for 4 hours, the cytokine of IFN-γ produced in CD4+ and CD8+ T cells were counted. The number of antigen-specific IFN-γ producing T cells significantly increased in group 6, suggesting that TTABP plus α-PD-L1 treatment induced a tumor-specific T cell response. We further profiled infiltrating leukocytes in the primary and the distant tumors. Flow cytometry measurements for group 6 showed a significant increase in tumor- infiltration of CD4+ and CD8+ T cells in both primary and distant tumors (**Fig S25c-f**, **Fig S27**). These results demonstrated TTABP-mediated prodrug plus α-PD-L1 treatment increased the infiltration of the effector T cells to treat the metastasis.

We also tested whether there was any *in vivo* toxicity by measuring the body weight of mice in each cohort (SI, **section 15**). The body weight experiment showed negligible side-effects (**Fig S28**). Furthermore, we compared H&E stained images of the major organs (heart, liver, spleen, lung, and kidney) from normal mice to those treated with TTAP NPs and light. Neither results displayed noticeable organ damage or inflammation lesions, suggesting that no obvious heart, liver, spleen, lung, or kidney dysfunction for the mice were induced by the photoactivatable process using TTAP NPs (**Fig S29**). Further, as shown in **table S16**, we did not observe abnormal results from the serum analysis experiments, which suggests that no observable unwanted inflammation was induced. Excrement from the mice 96 h after an IR 806 dye conjugated TTAP nanoparticle i.v. injection was also collected. Compared to the PBS-injected control group, we detected the fluorescence of the IR-806 dye signal in the excrement of mice in the nanoparticle treated group (**Fig S30**), suggesting that TTAP NPs can be cleared from the body through the fecal route. In addition, as shown in **Fig S31**, in addition to liver, the fluorescence was also observed at kidney at 10, 24, 48 hours and disappeared at 96 and 168 hours, suggesting the RGD-TTAP NPs may also be excluded from the body through kidney, which is similar to other nanoparticles 27, 28 (**Fig S31**). All of these results demonstrate that the as-designed TTAP NPs possess high biosafety and are highly biocompatible.

Finally, to achieve targeted tumor therapy, we covalently conjugated the cyclical Arg-Gly-Asp (cRGD) peptide on the surface of nanoparticles (RGD-TTAP NPs) to enhance their tumor targeting properties (SI**, section 16**). To verify the targeted tumor-killing effect of RGD-TTAP NPs *in vivo*, we utilized mice bearing a subcutaneous 4T1 tumor xenograft. To explore the best accumulation time-point of RGD-TTAP NPs in the tumor tissue, the 4T1 tumor-bearing mice were intravenously injected with IR806 fluorescence dye modified RGD-TTAP-19 NPs (IR806-RGD-TTAP NPs) and subjected to *in vivo* imaging at different time-points. As an additional control, the cRGD free nanoparticles (IR806-TTAP NPs) were also intravenously injected. The fluorescence at the tumor site increased gradually and reached a maximum level 24 h post-injection. After 48 h, the fluorescence intensity of IR806-RGD-TTAP NPs in the 4T1 tumor gradually

decreased. However, the IR806-TTAP NPs treated mice displayed a much weaker contrast between normal and tumor tissues. (**Fig S32b**) This result demonstrates that the cRGD peptide actually improved the nanoparticle targeting to the tumor in our system.

As the accumulation of IR806-RGD-TTAP NPs in the tumor reached its maximum at 24 h, we then examined the treatment effect of IR806-RGD-TTAP NPs accompanied by irradiation with LED (650 nm, 20 mW cm−2) 24 h post intravenous injection for 30 min. After such treatment, the therapeutic effects were assessed by monitoring changes in tumor volume (**Fig S32d**) as well as by hematoxylin and eosin (H&E) staining of the tumor tissues (**Fig S32f**). We only observed that the tumor growth in the treatment group 6 (IR806-RGD-TTAP NPs + *hv*) was remarkably suppressed. From the H&E staining analysis, the tumor tissue also showed clear necrosis, which indicates that IR806-RGD-TTAP NPs can be effectively activated by far red LED irradiation for intense anticancer effect.

In sum, photolytic reaction has powerful and important applications in numerous aspects of chemistry, materials as well as biology. Our discovery of long wavelength single photon driven TTAP overcomes the key problems (low effectiveness and high photodamage) in existing methods. This method is "LEGO"-like and highly modular. The light partners (the photosensitizers and the PPGs-X) can be energetically matched to adapt to the needs of a wide range of electromagnetic spectrum wavelengths and numerous chemical structures of photoremovable protecting groups, photolabile linkages, and a broad range of targeted molecules. Moreover, we exemplified the biological promise of TTAP via creating an ambient air-stable, ultra-small, water- soluble TTAP nanoparticle. Such nanoparticles achieve highly effective, ultra-low power, long wavelength single photon driven anticancer prodrug activation and, in turn, potentiated anti-tumor immunotherapeutic responses and promoted abscopal effects.

Declarations

Funding: G.H thanks for financial support provided by University of massachusetts-Medical School.

Author contributions: L.H. conducted the majority experiments, ran most of the data analysis, and wrote the manuscript. L.Z. ran a portion of *in vivo* cancer therapy experiments and helped to revise manuscript. Y.C. is responsible for flow cytometry testing and immune cell analysis. N. Y, L. W and Y. Z. contributed to cancer immunotherapy experiments indlucing isolation of tumors, lymphocyte extraction. K. H is responsible for characterization of nanoparticles including transmission electron microscopy and hydrodynamic particle size testing. G.H. conceived and supervised the project and experiments and wrote the manuscript.

Competing interests: G.H. and L.H. are inventors on a patent filed by UMMS currentlypending.

Data and materials availability: Experimental procedures, additional data, and analysis are included in the supplementary materials.

References

1. Klán, P., Šolomek, T., Bochet, C. G., Blanc, A., Givens, R., Rubina, M., Popik, V., Kostikov, A., Wirz, J., Photoremovable Protecting Groups in Chemistry and Biology: Reaction Mechanisms and Efficacy. *Rev.* **113**, 119–191 (2013).
2. Ravetz, B. D., Pun, A. B., Churchill, E. M., Congreve, D. N., Rovis, T., Campos, L. M., Photoredox catalysis using infrared light via triplet fusion upconversion. **565**, 343– 346 (2019).
3. Shao, Q., Xing, B., Photoactive molecules for applications in molecular imaging and cell *Chem. Soc. Rev*. **39**, 2835–2846 (2009).
4. Mitsunaga, M., Ogawa, M., Kosaka, N., Rosenblum, L. T., Choyke, P. L., Kobayashi, H., Cancer cell–selective in vivo near infrared photoimmunotherapy targeting specific membrane molecules. *Med.* **17**, 1685–1691 (2011).
5. Welsher, , Liu, Z., Sherlock, S. P., Robinson, J. T., Chen, Z., Daranciang, D., Dai, H., A route to brightly fluorescent carbon nanotubes for near-infrared imaging in mice. *Nat. Nano.* **4**, 773–780 (2009).
6. Richers, M. , Amatrudo, J. M., Olson, J. P., Ellis-Davies, G. C. R., Cloaked Caged Compounds: Chemical Probes for Two-Photon Optoneurobiology. *Angew. Chem. Int. Ed.* **56**, 193–197 (2017).
7. Carling, C.-J., Boyer, J.-C., Branda, N. R., Remote-Control Photoswitching Using NIR Light J.*Am. Chem. Soc.* **131**, 10838–10839 (2009).
8. Dong, H., Du, S.-R., Zheng, -Y., Lyu, G.-M., Sun, L.-D., Li, L.-D., Zhang, P.-Z., Zhang, C., Yan, C.-H., Lanthanide Nanoparticles: From Design toward Bioimaging and Therapy. *Chem. Rev.* **115**, 10725–10815 (2015).
9. Y., Feng, W., Yang, P., Huang, C., Li, F., The biosafety of lanthanide upconversion nanomaterials. *Chem. Soc. Rev.* **44**, 1509–1525 (2015).
10. Zhou, J., Liu, Q., Feng, , Sun, Y., Li, F., Upconversion Luminescent Materials: Advances and Applications. *Chem. Rev.* **115**, 395–465 (2015).
11. Zhao, J., Xu, K., Yang, , Wang, Z., Zhong, F., The triplet excited state of Bodipy: formation, modulation and application. *Chem. Soc. Rev.* **44**, 8904–8939 (2015).
12. Singh-Rachford, N., Castellano, F. N., Photon upconversion based on sensitized triplet– triplet annihilation. *Coord. Chem. Rev.* **254**, 2560–2573 (2010).
13. Huang, D., Sun, J., Ma, L., Zhang, C., Zhao, J., Preparation of ketocoumarins as heavy atom- free triplet photosensitizers for triplet–triplet annihilation upconversion. *Photobiol. Sci.* **12**, 872–882 (2013).
14. Hofbeck, , Yersin, H., The Triplet State of fac-Ir(ppy)3. *Inorg. Chem*. **49**, 9290–9299 (2010).
15. Ji, S., Wu, , Wu, W., Guo, H., Zhao, J., Ruthenium(II) Polyimine Complexes with a Long-Lived 3IL Excited State or a 3MLCT/3IL Equilibrium: Efficient Triplet Sensitizers for Low- Power Upconversion. *Angew. Chem. Int. Ed.* **50**, 1626–1629 (2011).
16. Cui, X., Zhao, J., Zhou, , Ma, J., Zhao, Y., Reversible photoswitching of triplet–triplet annihilation upconversion using dithienylethene photochromic switches. *J. Am. Chem. Soc.* **136**, 9256–9259

(2014).

17. DeForest, C. A., Anseth, K. S., Cytocompatible click-based hydrogels with dynamically tunable properties through orthogonal photoconjugation and photocleavage reactions. *Nat Chem.* **3**, 925–931 (2011).
18. Goswami, P., Syed, A., Beck, C. L., Albright, T. R., Mahoney, K. M., Unash, R., Smith, E. A., Winter, A. H., BODIPY-Derived Photoremovable Protecting Groups Unmasked with Green Light. *J. Am. Chem. Soc.* **137**, 3783–3786 (2015)
19. Hoelder, S., Clarke, A., Workman, P., Discovery of small molecule cancer drugs: successes, challenges and opportunities. *Mol. Oncol.* **6**, 155–176 (2012).
20. Muralidharan, A., Wyse, D., Smith, M. T., Analgesic efficacy and mode of action of a selective small molecule angiotensin II type 2 receptor antagonist in a rat model of prostate cancer-induced bone pain. *Pain Med.* **15**, 93–110 (2014).
21. Ivanenkov, A., Balakin, K. V., Lavrovsky, Y., Small Molecule Inhibitors of NF-□ B and JAK/STAT Signal Transduction Pathways as Promising Anti-Inflammatory Therapeutics. *Mini. Rev. Med. Chem.* **11**, 55–78 (2011).
22. Li, J., Mooney, J., Designing hydrogels for controlled drug delivery. *Nat. Rev. Mater.* **1**, 16071 (2016).
23. Mitragotri, S., Burke, A., Langer, R., Overcoming the challenges in administering biopharmaceuticals: formulation and delivery strategies. *Nat. Rev. Drug. Discov.* **13**, 655 (2014).
24. Bosch, , Dalla-Favera, R., Chronic lymphocytic leukaemia: from genetics to treatment. *Nat. Rev. Clin. Oncol.* doi.org/10.1038/s41571-019-0239-8 (2019).
25. Nam, J., Son, S., Park, K. S., Zou, , Shea, L. D., Moon, J. J., Cancer nanomedicine for combination cancer immunotherapy. *Nat. Rev. Mater.* **4**, 398–414 (2019).
26. Duan, X., Chan, C., Han, , Guo, N., Weichselbaum, R. R., Lin, W., Immunostimulatory nanomedicines synergize with checkpoint blockade immunotherapy to eradicate colorectal tumors. *Nat. Commun.* **10**, 1899 (2019).
27. Yu, ; Zheng, J. Clearance Pathways and Tumor Targeting of Imaging Nanoparticles. *ACS Nano* **9**, 6655 (2015).
28. Huang, ; Li, L.; Liu, T.; Hao, N.; Liu, H.; Chen, D.; Tang, F. The shape effect of mesoporous silica nanoparticles on biodistribution, clearance, and biocompatibility in vivo. ; *ACS Nano*, **5**, 5390 (2011)

Figures

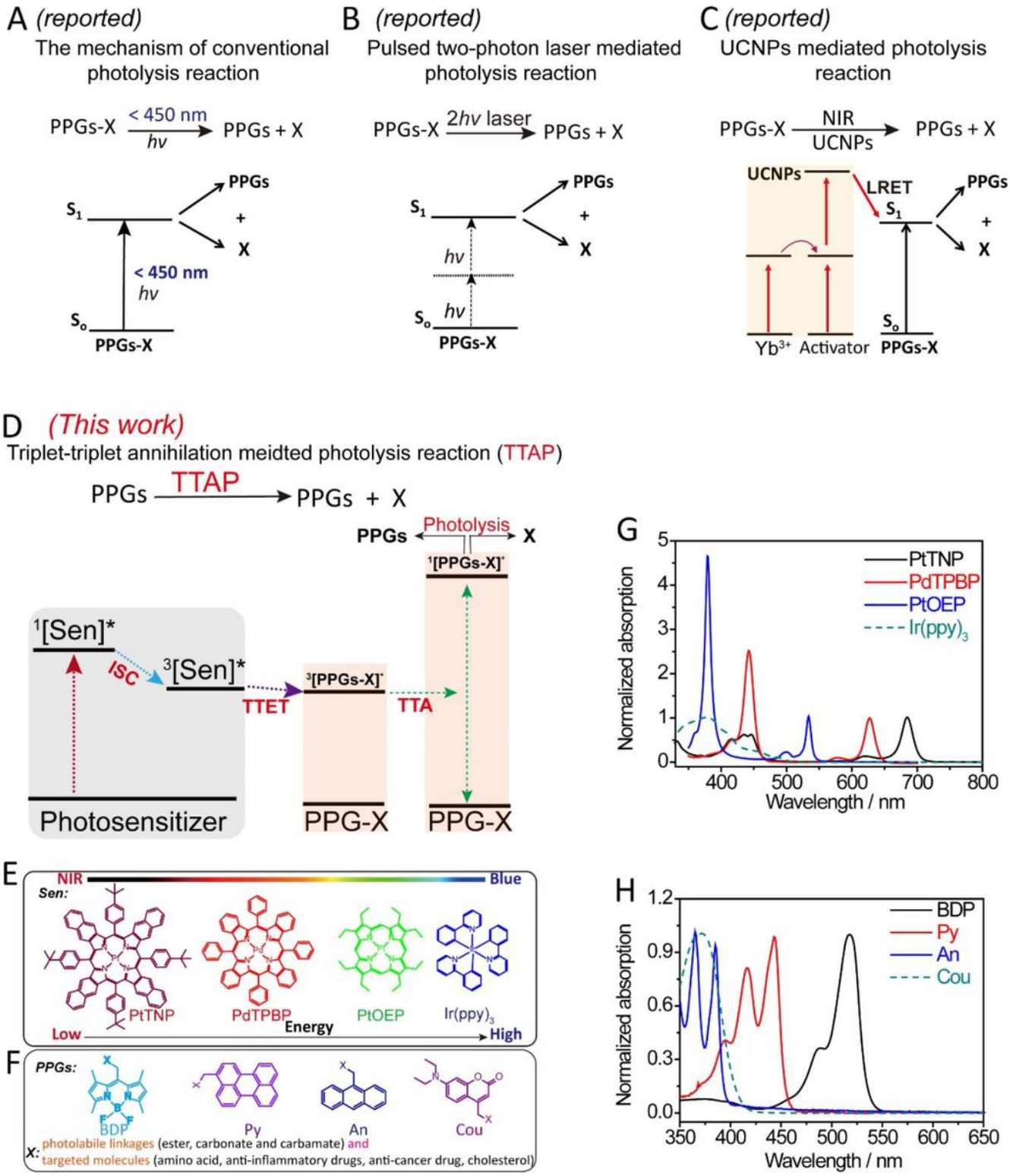

Figure 1

The mechanism of reported state-of-the-art photolytic reactions and the TTAP mechanism in this work. (a) The reported conventional short wavelength light direct activation (b) pulsed two photon laser strategy mechanism for photolytic reaction, hv: single photon, 2 hv: two photon; (c) The reported lanthanide ion doped upconversion nanoparticles (UCNPs) mediated photolytic reaction, LRET: luminescence resonance energy transfer; (d) The mechanism of triplet- triplet annihilation mediated

photolysis (TTAP, this work), ISC: intersystem crossing, TTET: triplet-triplet energy transfer, TTA: triplet-triplet annihilation 1[Sen]* : the singlet excited state of the photosensitizer; 3[Sen]* : the triplet excited state of the photosensitizer; PPGs: photoremovable protecting groups (BDP, Py, An and Cou), X: targeted molecules (amino acids, anti-inflammatory drugs, anti-cancer drug, cholesterol) and photolabile linkage (ester bond, carbonate, carbamate); (e) the molecular structures of photosensitizers, including PtTNP, PdTPBP, PtOEP and Ir(ppy)3; (f) The molecular structures of PPGs, including BDP, Py, An and Cou moieties. (g) The normalized UV-vis absorption spectra of Sen. (h) The normalized UV-vis absorption spectra of PPGs.

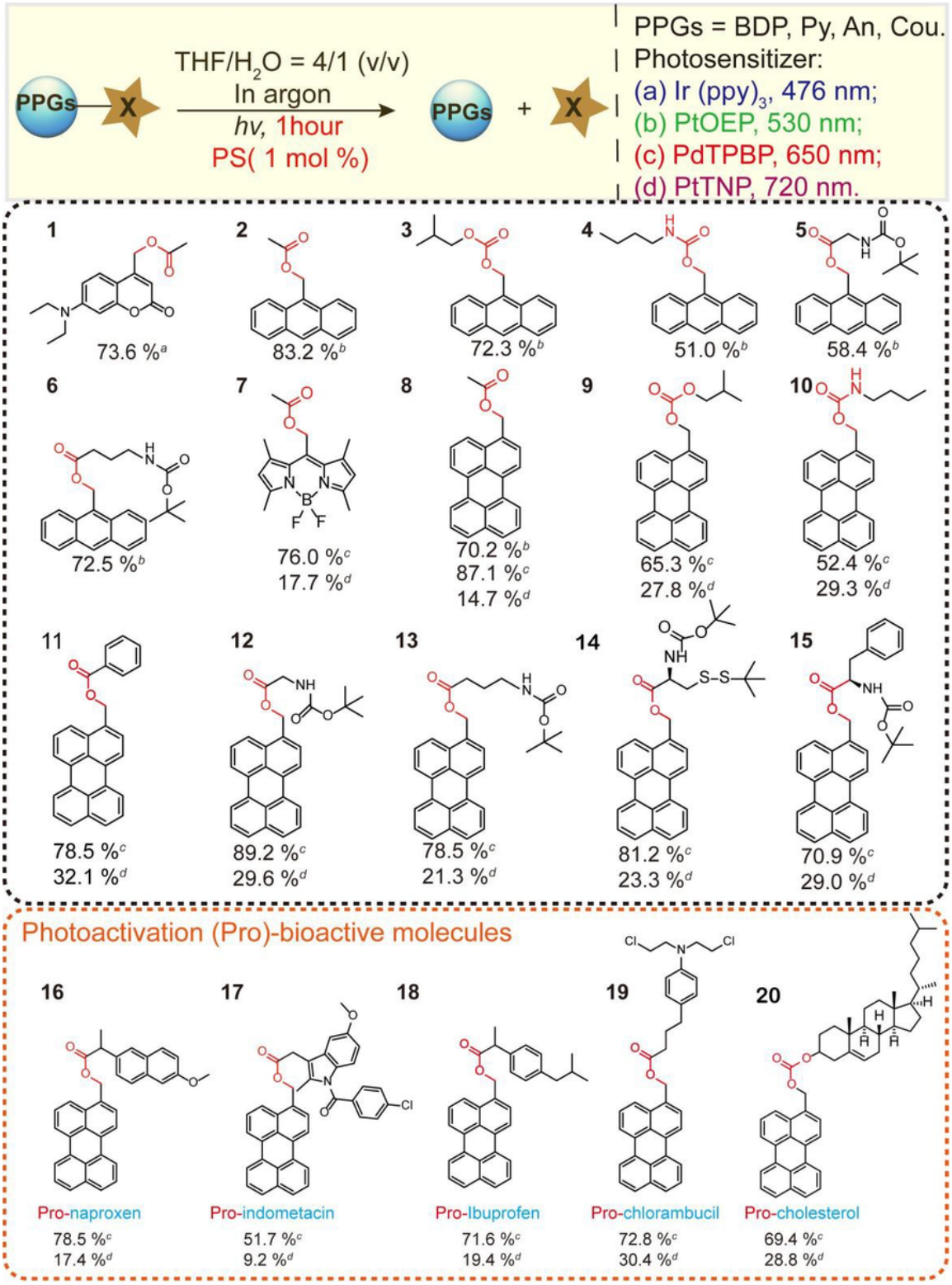

Figure 2

Triplet-triplet annihilation mediated photolytic reactions under diverse low power long wavelength LED irradiation. The superscripts (a-d) next to the reaction yields represent the sensitizers used and their respective operation light wavelengths.

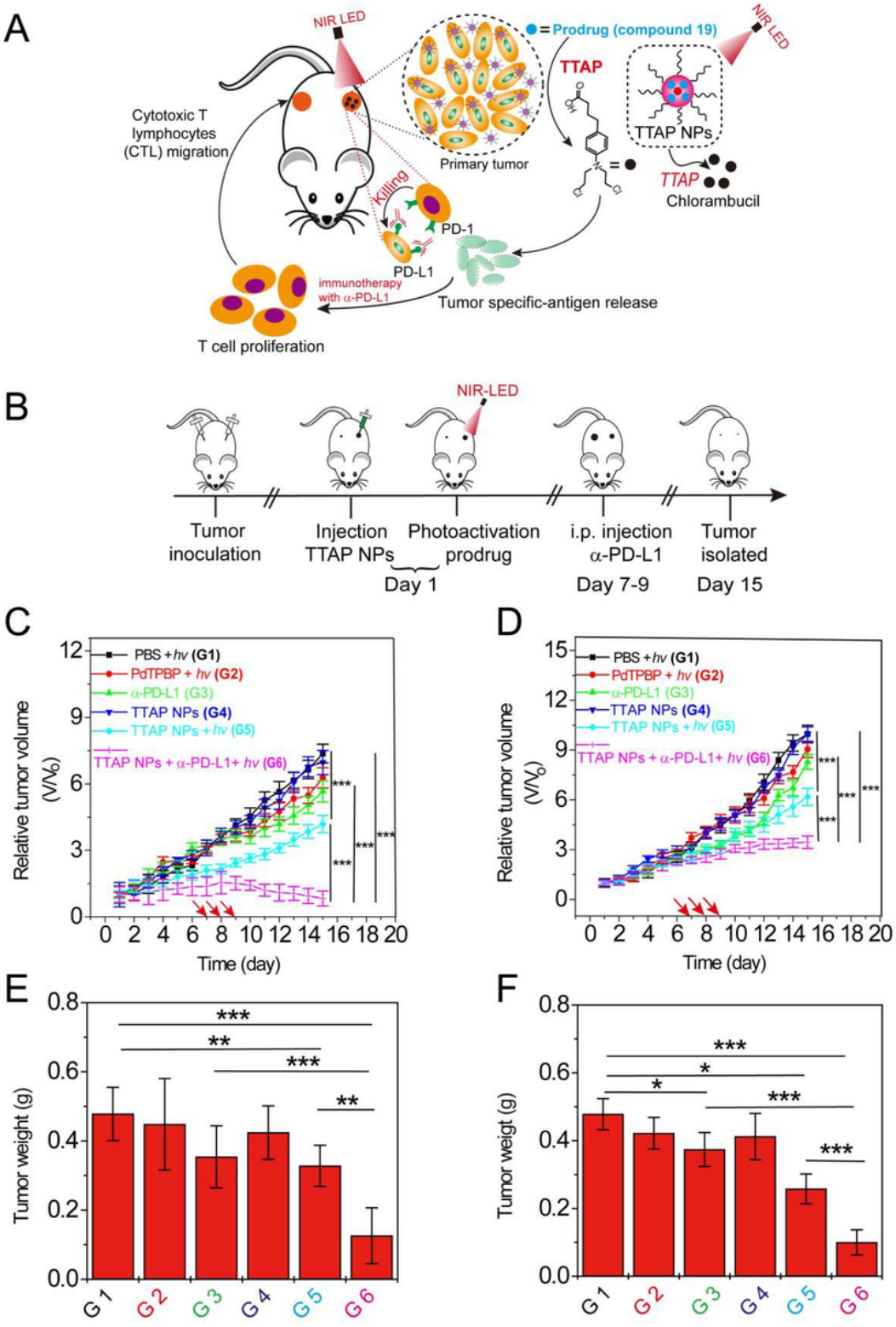

Figure 3

TTAP NPs mediated synergistic immunotherapy. (a) A schematic illustration of the in vivo study TTAP NPs mediated prodrug photoactivation with checkpoint blockade the □-PD-L1 antibody to realize synergistic immunotherapy in a bilateral model of 4T1 tumor bearing BALB/c mice, the right side tumor stands for (primary tumor), the left side tumor stands for (distant tumor or “metastatic tumor”); (b) A schematic illustration of the experimental immunotherapy process, the 4T1 cells were seeded at mice

right back and the left mice back, waiting for the right side tumor volume reached to 100 mm3, the TTAP NPs was intratumorally injected, then NIR LED (20 mW/cm2, 650 nm) illuminated the right side tumor; at 7 th, 8 th and 9 th, the □-PD-L1 was i.p. injected for mice (group 3 and group 6). (c) The growth curves of primary tumors; (d) The growth curves of distant tumors, the red arrow stands for i.p. injection □-PD-L1 for group 3 and group 6 at 7 th, 8 th and 9 th day. (e) The primary tumor weight and (f) the distant tumor weight. “G” is the abbreviation of group, values are means □ s.e.m. (n = 5 mice per group). *p < 0.05, **p < 0.01 and ***p < 0.001.

Supplementary Files

This is a list of supplementary files associated with this preprint. Click to download.

- NatureCommFormatSI.pdf